

Production and evolution path of dileptons at energies accessible to the HADES detectorK. Schmidt,¹ E. Santini,¹ S. Vogel,¹ C. Sturm,² M. Bleicher,¹ and H. Stöcker^{1,3,4}¹*Institut für Theoretische Physik, Goethe-Universität, Max-von-Laue-Str. 1, D-60438 Frankfurt am Main, Germany*²*Institut für Kernphysik, Goethe-Universität, Max-von-Laue-Str. 1, D-60438 Frankfurt am Main, Germany*³*Frankfurt Institute for Advanced Studies (FIAS), Ruth-Moufang-Str. 1, D-60438 Frankfurt am Main, Germany*⁴*GSI Helmholtzzentrum für Schwerionenforschung GmbH, Planckstrasse 1, D-64291 Darmstadt, Germany*

(Received 8 December 2008; published 24 June 2009)

Dilepton production in intermediate energy nucleus-nucleus collisions as well as in elementary proton-proton reactions is analyzed within the ultrarelativistic quantum molecular dynamics transport model. For C+C collisions at 1A GeV and 2A GeV the resulting invariant mass spectra are compared to recent HADES data. We find that the experimental spectrum for C+C at 2A GeV is slightly overestimated by the theoretical calculations in the region around the vector meson peak but fairly described in the low mass region, where the data are satisfactorily saturated by the Dalitz decay of the η meson and the Δ resonance. At 1A GeV an underestimation of the experimental data is found, pointing that at lower energies the low-mass region is not fully saturated by standardly parametrized Δ Dalitz decays alone. Furthermore, predictions for dilepton spectra for pp reactions at 1.25, 2.2, and 3.5 GeV and Ar+KCl reactions at 1.75A GeV are presented. The study is complemented by a detailed investigation of the role of absorption of the parent particles on the corresponding dilepton yields in the regime that has so far been probed by HADES.

DOI: [10.1103/PhysRevC.79.064908](https://doi.org/10.1103/PhysRevC.79.064908)

PACS number(s): 13.40.Hq, 24.10.Lx, 25.75.Dw

I. INTRODUCTION

Since the early 1990s experimental and theoretical efforts have been directed to the investigation of dilepton production in heavy-ion collisions [1–34]. Dileptons represent a particularly clean and penetrating probe of the hot and dense nuclear matter due to the fact that, once produced, they essentially do not interact with the surrounding hadronic matter. The analysis of the electromagnetic response of the dense and hot medium is tightly connected to the investigation of the in-medium modification of the vector-meson properties. Vector mesons can directly decay into a lepton-antilepton pair. One therefore aims to infer information on the modifications induced by the medium on specific properties of the vector meson, such as its mass and/or its width, from the invariant mass dilepton spectra.

A first generation of ultrarelativistic heavy-ion collision experiments performed in the 1990s observed an enhancement of dilepton production in heavy system at low invariant mass as compared to conventional hadronic cocktails and models [7, 11]. The enhancement could be later explained by the inclusion of an in-medium modified ρ meson. At that time two possible scenarios, a dropping of the ρ -meson mass according to the Brown-Rho scaling hypothesis [35] and the Hatsuda and Lee sum-rule prediction [36] or a “melting” of its spectral function as expected within many-body hadronic models [16, 17, 37, 38], have been offered in attempt to explain these data [12–15, 18]. If on the one side these experiments clearly showed the need for an inclusion of in-medium effects, on the other side it could not be decided, on the basis of the experimental data, whether the additional strength at lower invariant masses was due to a dropping of the vector-meson mass or to the broadening of its spectral function. A first answer in this direction came from the measurements performed by the NA60 Collaboration [24]. The data strongly favor the broadening over the dropping mass scenario. A similar conclusion is suggested by recent higher resolution CERES data [25].

At lower bombarding energies dileptons have been measured by the DLS Collaboration at BEVALAC [19]. The most striking result of the DLS experiment was an observed enhancement at lower invariant masses in nucleus-nucleus collisions at 1A GeV with respect to the corresponding theoretical spectra resulting from transport calculations [20–23]. Differing from the ultrarelativistic case, none of the in-medium scenarios that had successfully explained the ultrarelativistic heavy-ion collision data could account for the observed enhancement [20, 21] (this is known as the DLS puzzle). In the meanwhile the HADES spectrometer has been built at GSI with the aim of performing a systematic study of dilepton production in elementary, as well as heavy-ion reactions. First HADES data have recently been presented [26, 27], accompanied by a growing related theoretical activity [28–30, 32, 34]. Aim of this work is a detailed investigation of dilepton production in heavy-ion and elementary reactions at SIS energies.

The systems analyzed here have been chosen according to the HADES program. For those systems for which the HADES data and detector filter function are available a direct comparison to the data is performed. The additional calculations are given as predictions that can be compared to experimental data in the near future. The outline of the article is the following: After a brief survey of the ultrarelativistic quantum molecular dynamics (UrQMD) model and of the therein implemented dilepton production channels in Sec. II, proton-proton reactions are discussed in Sec. III, where the model calculations are compared to existing DLS data and predictions for the related projects of the HADES Collaboration, pp at 1.25, 2.2, and 3.5 GeV, are presented. In Sec. IV dilepton spectra for C+C collisions are shown. In Sec. V we turn to predictions for the forthcoming analysis of dilepton production in Ar+KCl collisions. Section VII is devoted to the study of the time evolution of the dilepton

emission and its connection with the various density regimes experienced in the course of the heavy-ion collision. Summary and concluding remarks are finally given in Sec. VIII.

II. THE MODEL

A. UrQMD

The analysis is performed within the microscopic UrQMD model, a nonequilibrium transport approach based on the quantum molecular dynamics concept [39–41]. The model allows for the production of all established meson and baryon resonances up to 2.2 GeV with all corresponding isospin projections and antiparticle states (taken from Ref. [42]). The collision term describes particle production by resonant excitation channels and, for higher energies, within a string fragmentation scheme. For dilepton production at SIS energies, the resonant production of neutral mesons is most important. Resonances also interact with all other particles given the collision criterion is met ($d < \sqrt{\sigma/\pi}$, with d being the distance of closest approach and σ being the cross section of the binary collision). Thus, reabsorption and collisional broadening is dynamically implemented. Note, however, that the model cannot feature the full quantum mechanical description of particle production and evolution in heavy-ion collisions. The model does not account for off-shell propagation of resonances and resonances are produced with vacuum spectral functions. The model allows the study of the full space-time evolution for all hadrons, resonances, and their decay products. This permits to explore the emission patterns of the resonances in detail and to gain insight into the origin of the resonances. UrQMD has been successfully applied to study light and heavy-ion reactions at SIS. Detailed comparisons of UrQMD with a large body of experimental data at SIS energies can be found in Ref. [43].

For further details of the model the reader is referred to Refs. [44,45]; the latest version (v2.3) is described in Ref. [46].

B. Meson production in UrQMD

In the UrQMD model the formation of most light mesons at low energies is modeled as a multistep process that proceeds via intermediate heavy baryon and meson resonances and their subsequent decay [47]. The probability for a resonance to decay into a specific channel is determined by the branching ratio, i.e., by the ratio between the partial decay width for the decay into the exit channel and the total decay width of the resonance, both of which depend on the resonance running mass. In the UrQMD model, the full decay width $\Gamma_{\text{tot}}(M)$ of a resonance is defined as the sum of all partial decay widths and depends on the mass of the excited resonance:

$$\Gamma_{\text{tot}}(M) = \sum_{br=(i,j)}^{N_{br}} \Gamma_{i,j}(\mu). \quad (1)$$

The partial decay widths $\Gamma_{i,j}(\mu)$ for the decay into the exit channel with particles i and j is given by:

$$\Gamma_{i,j}(\mu) = \Gamma_R^{i,j} \frac{\mu_R}{\mu} \left[\frac{\langle p_{i,j}(\mu) \rangle}{\langle p_{i,j}(\mu_R) \rangle} \right]^{2l+1} \frac{1.2}{1 + 0.2 \left[\frac{\langle p_{i,j}(\mu) \rangle}{\langle p_{i,j}(\mu_R) \rangle} \right]^{2l}}, \quad (2)$$

here μ_R denotes the pole mass of the resonance, $\Gamma_R^{i,j}$ its partial decay width into the channel i and j at the pole, and l the decay angular momentum of the exit channel; $\langle p_{i,j}(M) \rangle$ is the momentum of the decay products in the rest frame of the resonance. If the outgoing particles are stable particles with a well-defined mass, then $\langle p_{i,j} \rangle$ coincides with the standard momentum of the decay products in the rest frame of the resonance. If the outgoing particles are resonances, the width of their mass distribution is taken into account and $\langle p_{i,j} \rangle$ is determined as integral over the mass distribution of the respective resonance. For further details we refer the reader to Ref. [44]. The resonance parameters (pole masses and total and partial decay widths at the pole) are within the limits of Ref. [42]. However, in many cases only crude estimates for $\Gamma_R^{i,j}$ are given in Ref. [42]. For nonstrange baryon resonances, all masses, full widths, and decay probabilities used in UrQMDv2.3 are listed in Table I and have been fixed over the years.

Baryon resonances can be produced both in baryon-baryon and meson-baryon collisions. For the baryon-baryon cross sections an effective parametrization based on simple phase-space considerations is used; the cross section has the general form:

$$\sigma_{1,2 \rightarrow 3,4}(\sqrt{s}) \sim (2S_3 + 1)(2S_4 + 1) \frac{\langle p_{3,4} \rangle}{\langle p_{1,2} \rangle} \times \frac{1}{(\sqrt{s})^2} |\mathcal{M}(m_3, m_4)|^2. \quad (3)$$

The matrix element $|\mathcal{M}(m_3, m_4)|^2$ is assumed to have no spin dependence but may depend on the masses of the outgoing particles. In UrQMD, the excitation of nonstrange baryon resonances is subdivided into six classes: $NN \rightarrow N\Delta_{1232}$, $NN \rightarrow NN^*$, $NN \rightarrow N\Delta^*$, $NN \rightarrow \Delta_{1232}\Delta_{1232}$, $NN \rightarrow \Delta_{1232}N^*$, and $NN \rightarrow \Delta_{1232}\Delta^*$. Here the Δ_{1232} is explicitly listed, whereas higher excitations of the Δ resonance have been denoted as Δ^* . For each of these classes specific assumptions are made with regard to the form of the matrix element $|\mathcal{M}(m_3, m_4)|^2$; free parameters were tuned to experimental measurements when available. Form and values of the matrix element for each class can be found in Ref. [44]. The cross section depends also on the momenta of the in- and outgoing particles in the two-particle rest frame $\langle p_{i,j} \rangle$. Again, if the particles are resonances, the width of their mass distribution is taken into account on the determination of $\langle p_{i,j} \rangle$.

Meson-baryon collisions are treated as two-stage processes, i.e., first the meson is absorbed by a nucleon or a baryonic resonance forming a new resonance state with subsequent decay. Meson-baryon cross section are proportional to the partial decay width of the reverse process; for example, the total meson-baryon cross section for nonstrange particles is

TABLE I. Masses, widths, and branching ratios for nonstrange baryon resonances in UrQMDv2.3. Masses are given in GeV and the widths in MeV.

Resonance	Mass	Width	$N\pi$	$N\eta$	$N\omega$	$N\rho$	$N\pi\pi$	$\Delta_{1232}\pi$	$N_{1440}^*\pi$	ΛK	ΣK	$f_0 N$	$a_0 N$
N_{1440}^*	1.440	350	0.65				0.10	0.25					
N_{1520}^*	1.515	120	0.60			0.15	0.05	0.20					
N_{1535}^*	1.550	140	0.60	0.30			0.05		0.05				
N_{1650}^*	1.645	160	0.60	0.06		0.06	0.04	0.10	0.05	0.07	0.02		
N_{1675}^*	1.675	140	0.40					0.55	0.05				
N_{1680}^*	1.680	140	0.60			0.10	0.10	0.15	0.05				
N_{1700}^*	1.730	150	0.05			0.20	0.30	0.40	0.05				
N_{1710}^*	1.710	500	0.16	0.15		0.05	0.21	0.20	0.10	0.10	0.03		
N_{1720}^*	1.720	550	0.10			0.73	0.05			0.10	0.02		
N_{1900}^*	1.850	350	0.30	0.14	0.39	0.15				0.02			
N_{1990}^*	1.950	500	0.12			0.43	0.19	0.14	0.05	0.03		0.04	
N_{2080}^*	2.000	550	0.42	0.04	0.15	0.12	0.05	0.10		0.12			
N_{2190}^*	2.150	470	0.29			0.24	0.10	0.15	0.05	0.12			
N_{2220}^*	2.220	550	0.29		0.05	0.22	0.17	0.20		0.12			
N_{2250}^*	2.250	470	0.18			0.25	0.20	0.20	0.05	0.12			
Δ_{1232}	1.232	115	1.00										
Δ_{1600}^*	1.700	350	0.10					0.65	0.25				
Δ_{1620}^*	1.675	160	0.15			0.05		0.65	0.15				
Δ_{1700}^*	1.750	350	0.20			0.25		0.55					
Δ_{1900}^*	1.840	260	0.25			0.25		0.25	0.25				
Δ_{1905}^*	1.880	350	0.18			0.80		0.02					
Δ_{1910}^*	1.900	250	0.30			0.10		0.35	0.25				
Δ_{1920}^*	1.920	200	0.27					0.40	0.30	0.03			
Δ_{1930}^*	1.970	350	0.15			0.22		0.20	0.28	0.15			
Δ_{1950}^*	1.990	350	0.38			0.08		0.20	0.18	0.12			0.04

given by

$$\begin{aligned}
 \sigma_{\text{tot}}^{MB}(\sqrt{s}) &= \sum_{R=\Delta, N^*} \langle j_B, m_B, j_M, m_M \| J_R, M_R \rangle \\
 &\times \frac{2S_R + 1}{(2S_B + 1)(2S_M + 1)} \\
 &\times \frac{\pi}{P_{\text{CMS}}^2} \frac{\Gamma_{R \rightarrow MB} \Gamma_{\text{tot}}}{(M_R - \sqrt{s})^2 + \frac{\Gamma_{\text{tot}}^2}{4}} \quad (4)
 \end{aligned}$$

with the total and partial \sqrt{s} -dependent decay widths Γ_{tot} and $\Gamma_{R \rightarrow MB}$. Meson final-state interactions are assumed to be mediated by the re-excitation of resonances, according to Eq. (4).

The cross section for a specific exit channel $MB \rightarrow R \rightarrow M'B'$ can be obtained by replacing the total width Γ_{tot} in Eq. (4) by the respective partial decay width $\Gamma_{R \rightarrow M'B'}$. This implies that the full M' -production cross section in MB reactions is modeled as an incoherent sum over all resonances of Breit-Wigner type amplitudes. The same approximation has been used in other works [23,48]. The resonance R , however, enters as a dynamical degree of freedom in the UrQMD model; in particular, between creation in $MB \rightarrow R$ and decay $R \rightarrow M'B'$ the resonance is propagated and, in medium, can undergo final-state interactions. Further details can be found in Ref. [44]. Analogous considerations yield for meson production in NN collisions.

A comparison between the exclusive and inclusive cross sections for the production of neutral $\pi^0, \eta, \rho^0, \omega$ mesons

in pp reactions obtained within the UrQMD model and experimental data can be found in Ref. [45]. The production of the η and the resonant exclusive production of the ρ^0 meson, particularly important at low energies, will be discussed more in detail in the following sections.

1. Isospin asymmetry in η production

In the analysis of dilepton spectra in nucleus-nucleus collisions performed with the UrQMD model in Ref. [21], the dilepton yield originating from the η Dalitz decay was found about a factor of 2 lower than that in Ref. [20] and Ref. [49]. In the latter, the η channel had been determined from the measurements of the TAPS Collaboration. As already anticipated in Ref. [21], the discrepancy could be attributable to the fact that the asymmetry in the η production in pp and pn reactions (η production cross sections in pn reactions are about a factor of 5 higher than in the pp reaction) had been neglected in the calculations. Such asymmetry has been introduced for the present analysis (see Fig. 1). The inclusion has been performed, as in Ref. [51], at the level of the production cross section of the $N^*(1535)$ resonance. For the C+C reactions under study the η multiplicity obtained within the UrQMD model is now consistent with the value measured by the TAPS Collaboration [52], as shown in Fig. 2. The experimental constraint imposed by the TAPS measurements on the η Dalitz contribution to the dilepton spectra in nucleus-nucleus collisions is thus respected by our calculations. Especially for

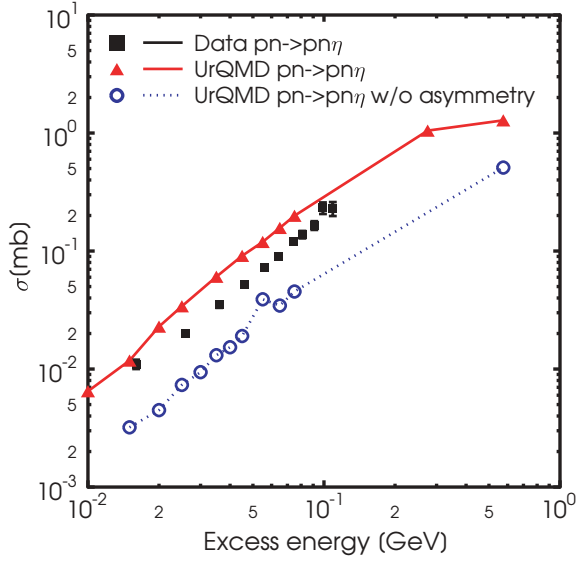


FIG. 1. (Color online) The η -production cross section from pn reactions as a function of the excess energy. The UrQMD results obtained with the novel introduction of the isospin asymmetry in the η -production cross section (triangles) are compared to experimental data [50]. The circles refer to calculations that neglect such asymmetry and are shown for completeness.

C+C collisions at 2A GeV, this is very important because, as we will see, the η decay plays an important role in determining the spectra in the low-mass region.

The energy dependence of the exclusive $pn \rightarrow pn\eta$ cross section as shown in Fig. 1 provides a reasonable description of the data; however, a finer parametrization, as, e.g., in Ref. [32], might be required in future studies of dilepton production in

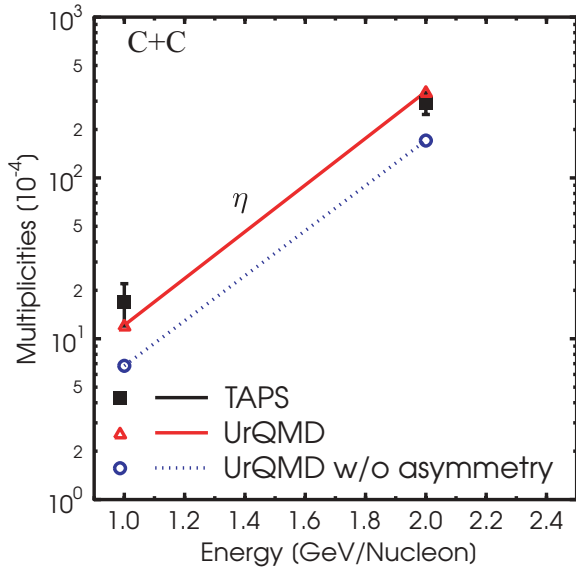


FIG. 2. (Color online) Average η multiplicity in C+C reactions at 1A GeV and 2A GeV from UrQMD (triangle) in comparison to the values reported by the TAPS Collaboration [52]. The circles refer to the standard calculations that neglect the isospin asymmetry in the η -production cross section and are shown for completeness.

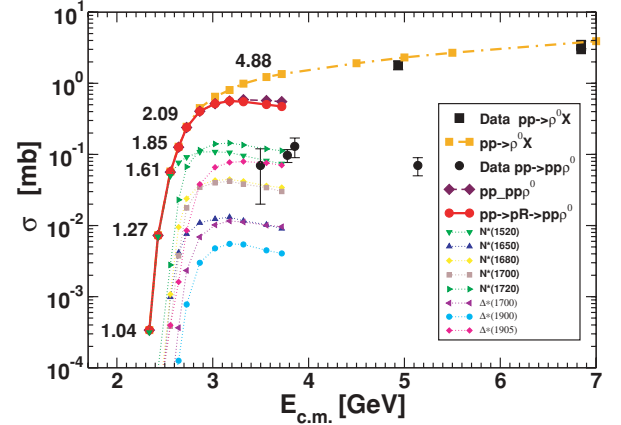


FIG. 3. (Color online) Cross sections for ρ^0 meson production in pp collisions. Calculations are shown for inclusive ($pp \rightarrow \rho^0 X$) and exclusive ($pp \rightarrow pp\rho^0$) in comparison to experimental data [53]. The contribution of the most important resonances to the resonant exclusive production is additionally shown.

elementary pn reactions. Especially for those cases where fixing the η contribution with high precision is mandatory to achieve a unique interpretation of the experimental data in the low-mass region a retuning is necessary. However, pn reactions are not the major subject of this work, and the new prescription used here for the treatment of η production provides sufficient robustness for the dilepton studies presented in the next sections.

2. ρ production

Figure 3 shows the cross sections for the inclusive ($pp \rightarrow \rho^0 X$) and exclusive ($pp \rightarrow pp\rho^0$) production of the neutral ρ meson in pp collisions, in comparison with experimental data from Ref. [53]. The points corresponding to the energies scanned by the DLS pp program are labeled by the corresponding laboratory energies to simplify the readability of the figure in view of later discussions. The resonant contribution to the exclusive production, important at the energies relevant for this work, is separately shown. Moreover, the contribution of the most important resonance is explicitly shown. To specify the order of the relative scale, the contribution of some of the less important resonance is also shown. The full list of resonances that couple to the ρ meson in the UrQMD model is given in Table I together with the values of the respective branching ratios in the $N\rho$ decay channel as used in UrQMD v2.3. Some of the values for the branching ratios differ from the ones used in UrQMD v1.0 [21,44]. However, the same values are used since UrQMD v1.1. Above the threshold for meson production by string fragmentation and decay, the $pp \rightarrow pp\rho^0$ reaction channel is additionally populated by processes involving strings.

Unless explicitly specified, in the following we will discuss in terms of laboratory energies. One observes that in collisions at laboratory energies of 1.04–2.09 GeV the ρ -meson production is determined by the excitation of Δ^* and N^* resonances in reactions $pp \rightarrow pN^*$ and $pp \rightarrow p\Delta^*$

and the inclusive production of the ρ meson coincides with the exclusive production. In particular, the latter is practically saturated by the contribution of the $N^*(1520)$ resonance up to beam energies of 1.61 GeV. On the contrary, at 4.88 GeV, the inclusive production dominates by far the exclusive production. The first data points on inclusive production are well reproduced by the model but are far away from the energies spanned by the DLS and the HADES experiments. The exclusive production, on the contrary, is systematically overestimated.

Poor and often contradictory experimental information is available on the production cross sections of N^* and Δ^* resonances. For example, in the case of the $N^*(1520)$ resonance a reduction of the cross section currently used in UrQMD by a factor of 3 is possible in comparison to the experimental data [53] and results even in a smaller value of the weighted least-mean-square for that specific channel. We will discuss this possible source of indetermination more in detail in Sec. VI.

C. Dilepton radiation in UrQMD

In UrQMD, dilepton pairs are generated from the mesonic Dalitz decays $\pi^0 \rightarrow \gamma e^+ e^-$, $\eta \rightarrow \gamma e^+ e^-$, $\eta' \rightarrow \gamma e^+ e^-$, and $\omega \rightarrow \pi^0 e^+ e^-$; the direct decay of the ρ , ω , and ϕ vector mesons; and the Dalitz decay of the Δ resonance. These are the dominant contributions to the dilepton spectrum at GSI-SIS energies. Assuming, as done in the present approach, a sharp factorization for the processes $R \rightarrow NV \rightarrow Ne^+ e^-$ according to $R \rightarrow NV$ with subsequent decay $V \rightarrow Ne^+ e^-$, the Dalitz decay of higher-order resonances can be neglected. Due to complications with bremsstrahlung and double counting with the Δ Dalitz decay (an issue recently discussed) bremsstrahlung contributions are not calculated either.

Decays of the form, with P being a pseudoscalar meson and V a vector meson,

$$P \rightarrow \gamma e^+ e^-, \quad V \rightarrow P e^+ e^- \quad (5)$$

can be decomposed into the corresponding decays into a virtual photon γ^* , $P \rightarrow \gamma \gamma^*$, $V \rightarrow P \gamma^*$, and the subsequent decay of the photon via electromagnetic conversion, $\gamma^* \rightarrow e^+ e^-$ [54–56]:

$$\frac{d\Gamma_{P \rightarrow \gamma e^+ e^-}}{dM^2} = \Gamma_{P \rightarrow \gamma \gamma^*} \frac{1}{\pi M^4} M \Gamma_{\gamma^* \rightarrow e^+ e^-}, \quad (6)$$

$$\frac{d\Gamma_{V \rightarrow P e^+ e^-}}{dM^2} = \Gamma_{V \rightarrow P \gamma^*} \frac{1}{\pi M^4} M \Gamma_{\gamma^* \rightarrow e^+ e^-}, \quad (7)$$

where M is the mass of the virtual photon or, equivalently, the invariant mass of the lepton pair. The internal conversion probability of the photon is given by:

$$M \Gamma_{\gamma^* \rightarrow e^+ e^-} = \frac{\alpha}{3} M^2 \sqrt{1 - \frac{4m_e^2}{M^2}} \left(1 + \frac{2m_e^2}{M^2}\right) \quad (8)$$

with m_e being the electron mass. The widths $\Gamma_{P \rightarrow \gamma \gamma^*}$ and $\Gamma_{V \rightarrow P \gamma^*}$ can be related to the corresponding radiative widths

$\Gamma_{P \rightarrow 2\gamma}$ and $\Gamma_{V \rightarrow P\gamma}$:

$$\Gamma_{P \rightarrow \gamma \gamma^*} = 2 \Gamma_{P \rightarrow 2\gamma} \left(1 - \frac{M^2}{m_P^2}\right)^3 |F_{P\gamma\gamma^*}(M^2)|^2, \quad (9)$$

$$\Gamma_{V \rightarrow P\gamma^*} = \Gamma_{V \rightarrow P\gamma} \left[\left(1 + \frac{M^2}{m_V^2 - m_P^2}\right)^2 - \left(\frac{2m_V M}{m_V^2 - m_P^2}\right)^2 \right]^{3/2} |F_{VP\gamma^*}(M^2)|^2, \quad (10)$$

where m_P and m_V are the masses of the pseudoscalar and vector meson, respectively, and $F_{P\gamma\gamma^*}(M^2)$, $F_{VP\gamma^*}(M^2)$ denote the form factors with $F_{P\gamma\gamma^*}(0) = F_{VP\gamma^*}(0) = 1$. The factor of 2 in Eq. (9) occurs due to the identity of the two photons in the $P \rightarrow 2\gamma$ decay. The form factors can be obtained from the vector-meson dominance model (VMD). In the present calculations the following parametrizations are employed [15,54]:

$$F_{\pi^0}(M^2) = 1 + b_{\pi^0} M^2, \quad (11)$$

$$F_{\eta}(M^2) = \left(1 - \frac{M^2}{\Lambda_{\eta}^2}\right)^{-1},$$

$$|F_{\omega}(M^2)|^2 = \frac{\Lambda_{\omega}^2 (\Lambda_{\omega}^2 + \gamma_{\omega}^2)}{(\Lambda_{\omega}^2 - M^2)^2 + \Lambda_{\omega}^2 \gamma_{\omega}^2},$$

$$|F_{\eta'}(M^2)|^2 = \frac{\Lambda_{\eta'}^2 (\Lambda_{\eta'}^2 + \gamma_{\eta'}^2)}{(\Lambda_{\eta'}^2 - M^2)^2 + \Lambda_{\eta'}^2 \gamma_{\eta'}^2}$$

with $b_{\pi^0} = 5.5 \text{ GeV}^{-2}$, $\Lambda_{\eta} = 0.72 \text{ GeV}$, $\Lambda_{\omega} = 0.65 \text{ GeV}$, $\gamma_{\omega} = 0.04 \text{ GeV}$, $\Lambda_{\eta'} = 0.76 \text{ GeV}$, and $\gamma_{\eta'} = 0.10 \text{ GeV}$. In Eq. (11) the abbreviations F_P and F_V have been used to denote respectively $F_{P\gamma\gamma^*}$ and $F_{VP\gamma^*}$.

The width for the direct decay of a vector meson $V = \rho^0, \omega, \phi$ to a dilepton pair varies with the dilepton mass like M^{-3} according to [15]:

$$\Gamma_{V \rightarrow e^+ e^-}(M) = \frac{\Gamma_{V \rightarrow e^+ e^-}(m_V)}{m_V} \frac{m_V^4}{M^3} \sqrt{1 - \frac{4m_e^2}{M^2}} \left(1 + \frac{2m_e^2}{M^2}\right) \quad (12)$$

with $\Gamma_{V \rightarrow e^+ e^-}(m_V)$ being the partial decay width at the meson pole mass.

The decomposition of the $\Delta \rightarrow Ne^+ e^-$ decay into the $\Delta \rightarrow N\gamma^*$ decay and subsequent conversion of the photon leads to the following expression for the differential decay width:

$$\frac{d\Gamma_{\Delta \rightarrow Ne^+ e^-}}{dM^2} = \frac{\alpha}{3\pi M^2} \Gamma_{\Delta \rightarrow N\gamma^*}. \quad (13)$$

Here the electron mass has been neglected. The decay width into a massive photon reads [3]:

$$\Gamma_{\Delta \rightarrow N\gamma^*}(M_{\Delta}, M) = \frac{\lambda^{1/2}(M^2, m_N^2, M_{\Delta}^2)}{16\pi M_{\Delta}^2} m_N \times [2\mathcal{M}_t(M, M_{\Delta}) + \mathcal{M}_l(M, M_{\Delta})], \quad (14)$$

where the kinematic function λ is defined by $\lambda(m_A^2, m_1^2, m_2^2) = [m_A^2 - (m_1 + m_2)^2][m_A^2 - (m_1 - m_2)^2]$ and M_{Δ} is the

resonance running mass. The matrix elements \mathcal{M}_t and \mathcal{M}_l are taken from Ref. [3]. The coupling constant g appearing in the expression for \mathcal{M}_t and \mathcal{M}_l has been chosen as $g = 5.44$, to reproduce the value of the radiative decay width, as done, e.g., in Ref. [57]. Note, that recently a more sophisticated parametrization of the Δ decay width has been derived [58]. However, the differences to the current parametrization are small (in the mass range with the largest difference it is on the order of 30% for the total spectra) and therefore the widely used formulas presented above have been applied.

D. Shining method

The “shining” method (also called time integration method) was introduced in Ref. [8] and Ref. [59] and assumes that a resonance can continuously emit dileptons over its whole lifetime. The dilepton yield is obtained by integration of the dilepton emission rate over time, taking the collisional broadening of each individual parent resonance into account:

$$\frac{dN_{e^+e^-}}{dM} = \frac{\Delta N_{e^+e^-}}{\Delta M} = \sum_{j=1}^{N_{\Delta M}} \int_{t_i^j}^{t_f^j} dt \frac{\Gamma_{e^+e^-}(M)}{\gamma \Delta M}. \quad (15)$$

Here $\Gamma_{e^+e^-}(M)$ is the electromagnetic decay width of the considered resonance defined in (12)–(14) and $t = t_i$ (t_f) the time at which the resonance appeared in (disappeared from) the system. Thus, even resonances that formally do not decay but are absorbed in another process (e.g., scattering with a proton) still emit dileptons depending on the time-span between their creation and annihilation.

For the calculations applying the “shining” method the whole time evolution of the collision is reconstructed. Each resonance is followed from the production time t_i to a final time t_f at which the resonance decays or is reabsorbed. The reabsorption cross sections are calculated via either the principle of detailed balance or the additive quark model. For more details regarding the interactions in the UrQMD model please refer to Refs. [44,45]. We implement the shining method for the short-lived vector mesons ρ and ω and the baryonic resonance Δ . Also note that for the analysis shown here, we implement no explicit in-medium treatment for dilepton production. The inclusion of scattering between the particles, however, accounts for collisional broadening dynamically.

In an alternative method, dileptons have been extracted at the point of decay of the resonances [29]. The dilepton yield is calculated at the decay vertex from the branching ratio. Thus, in this method the contribution to the dilepton yield of the reabsorbed resonances is neglected. However, as shown in Ref. [33] this contribution is small. A detailed comparison between the two methods can be found later in Sec. IV, Fig. 7. Note that for all calculations except the one shown in Sec. IV, Fig. 7, the shining method has been applied.

III. ELEMENTARY REACTIONS

A. Comparison to DLS measurements

Before addressing heavy-ion collisions we consider dilepton production in elementary reactions. The latter are very

important to gain a better understanding of the various processes contributing to the dilepton production and of their relative weights. Note, however, that the model does not describe dilepton production correctly in quantum-mechanical terms. It does not account for quantum-mechanical interferences between the various subprocesses producing dileptons. However, a comparison within the same model between elementary reactions and heavy-ion reactions is still a valuable analysis to be done and thus will be presented in the following section. In the energy range of interest for this work there exist measurements from the DLS [60] and HADES Collaboration.

Differential dilepton cross sections have been calculated with the present model for pp reactions at beam energies of 1.04, 1.27, 1.61, 1.85, 2.09, and 4.88 GeV. The results are presented in Fig. 4 in comparison to the DLS data [60]. To perform the comparison, the DLS acceptance filter and mass resolution have been included. For collisions at 1.04–2.09 GeV the agreement with the available data is generally reasonable in the region $M \leq 0.45$ GeV, where the π^0 , Δ , and η Dalitz decays dominate, whereas a systematic overestimation of the data is observed at higher masses. Especially at 2.09 GeV a clear overestimation of the dilepton cross section around the vector-meson peak is present, a result that is analogous to the findings of Ref. [32]. This might be due to an insufficient modeling of the production rate of high-mass resonances in $pp \rightarrow pN^*$, $pp \rightarrow p\Delta^*$ collisions. At bombarding energy of 4.88 GeV an inversion of this trend is observed and data are underestimated by the model calculations in the low invariant mass region but well described in the vector-meson region. This is not a contradiction. The main difference lies in the fact that at 4.88 GeV the exclusive production of the ρ meson does not affect significantly the inclusive production. The latter, on the other side, determines the ρ -meson yields in the reactions at 1.04–2.9 GeV.

B. Predictions for HADES

The HADES physic program includes measurement of pp reactions at 1.25, 2.2, and 3.5 GeV that we want to discuss here. In Fig. 5, UrQMD calculations for the three energies are presented. The beam energy $E = 1.25$ GeV is below the $pp \rightarrow pp\eta$ threshold and is therefore optimal for studying the contribution from Δ Dalitz. For $M > 0.45$ GeV a noticeable contribution from $\rho^0 \rightarrow e^+e^-$ is visible. This result differs from other calculations [32], where the contribution from the direct decay of the ρ meson is not seen at the lowest energy. This is due to the omission of an explicit treatment of ρ -meson production via resonant mechanism in Ref. [32], where a simplified parametrization of the $pp \rightarrow \rho X$ (vacuum) cross section of the form $\sigma(pp \rightarrow \rho X) \sim \int 2.2 [\frac{s}{s_0(M)} - 1]^{1.47} [\frac{s}{s_0(M)}]^{-1.1} A(M) dM$ has been employed. Here $A(M)$ denotes the meson spectral function and the integration is performed within the appropriate kinematical limits. Close to the physical threshold for ρ -meson production, $\sqrt{s}_{\text{th}} = 2m_N + 2m_\pi$, such omission results in smaller values of the cross section than those of this work and of other resonance model based approaches (see, e.g., Refs. [23,51,61]).

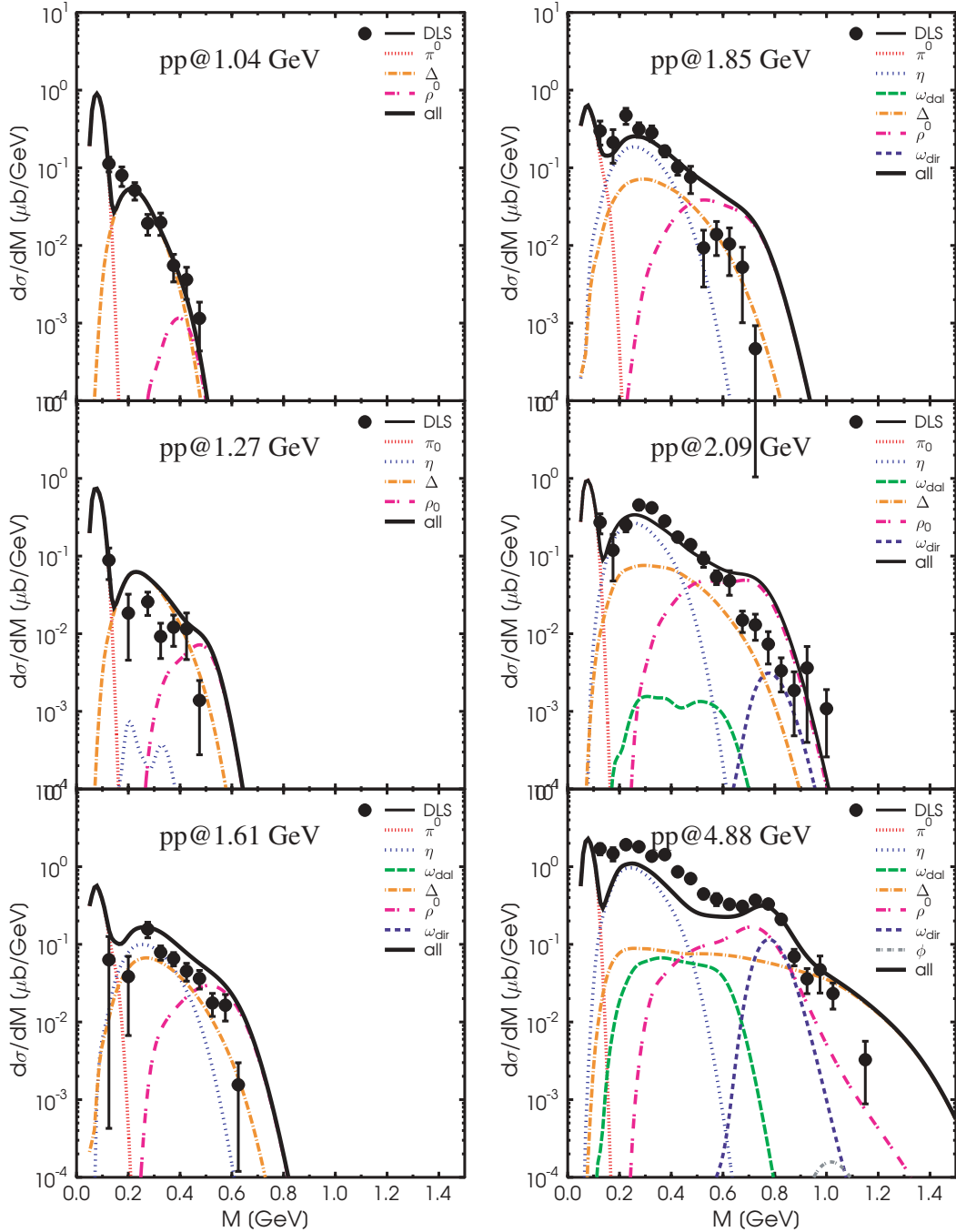


FIG. 4. (Color online) UrQMD model calculations for dilepton spectra from pp reactions at 1.04, 1.27, 1.61, 1.85, 2.09, and 4.88 GeV in comparison to the DLS data [60], including the DLS acceptance filter and mass resolution. The different color lines display individual channels in the transport calculation, as indicated in the legend.

In our model, this contribution arises naturally due to the possibility for baryonic resonances to decay into ρ . At rather low energies, this leads to the emission of a ρ meson with a mass distribution strongly biased by energy constraints. Here, the ρ mesons originates in particular from the decay of the $N^*(1520)$ resonance. For this chain the threshold is only $M = 2m_\pi$ and not m_ρ^{pole} . Early investigations on the role of the $N^*(1520)$ resonance for subthreshold ρ -meson production were performed in Refs. [22,57,62].

For higher beam energies all decays are possible as for the nucleus nucleus system. Both for 2.2 and 3.5 GeV the dilepton spectra in the lower mass regime are dominated by the long-lived resonances and the Δ resonance. For higher masses the direct decay of the ρ meson becomes more important and the double peak shape of the e^+e^- pairs originating from ρ is visible. At a beam energy of 3.5 GeV the contribution from the direct ω decay leads to a visible peak in the dilepton spectrum at $M \approx 0.8$ GeV.

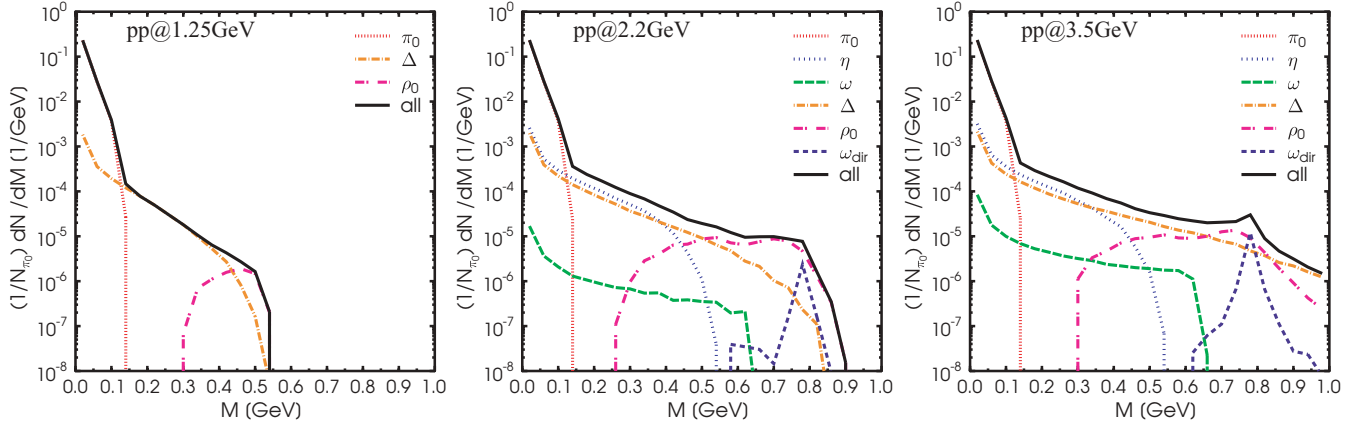


FIG. 5. (Color online) UrQMD model calculations for dilepton spectra from $p + p$ collisions at beam energies of 1.25 GeV (left panel), 2.2 GeV (middle panel), and 3.5 GeV (right part). The different color lines display individual channels from the transport calculation, as indicated in the legend.

IV. DILEPTON YIELDS IN C+C COLLISIONS

In this section we present calculations for dilepton spectra in minimum bias C+C reactions at 1.0A GeV and 2.0A GeV and compare them to the data resulting from the measurements performed by the HADES Collaboration [26,27]. To make the comparison with the experimental data, the filter function provided by the HADES Collaboration has been implemented [26,27]. In agreement with the treatment of the experimental data, dilepton events with opening angle $\Theta_{e^+e^-} \leq 9^\circ$ have been rejected and the spectra have been normalized to the mean π^0 multiplicity.

We first discuss the results obtained applying the “shining” method for the extraction of the dilepton yield and address Fig. 6, where the contributions to the spectra of the different channels are additionally explicitly shown. Both spectra are dominated by the π^0 decay for invariant masses $M \leq m_\pi$.

In the case of C+C at 2A GeV the η and Δ Dalitz decays dominate for $m_\pi < M \leq 0.5$ GeV with comparable magnitude. The present result for the Δ Dalitz contribution to the spectra is quantitatively similar to the result of Ref. [32], whereas in Refs. [30] and [34] a smaller contribution was found. For an explanation on the different treatments of the Δ Dalitz decay the reader is referred to the original publications. The direct decay of the ρ meson start to play a sizable role for $M \geq 0.5$ GeV. Due to the rapid decrease of the Δ Dalitz contribution, the relative importance of the ρ -meson direct decay channel grows with increasing invariant mass, from being at first comparable to the Δ Dalitz to becoming the dominant contribution in the region of the vector-meson peak. The low invariant mass region of the spectrum ($M < 0.5$ GeV) is successfully described by the UrQMD calculations. However, an overestimation of the data is observed at higher masses. A qualitatively analogous result has been found in the analysis of Ref. [32], where the “vacuum” calculation for C+C at

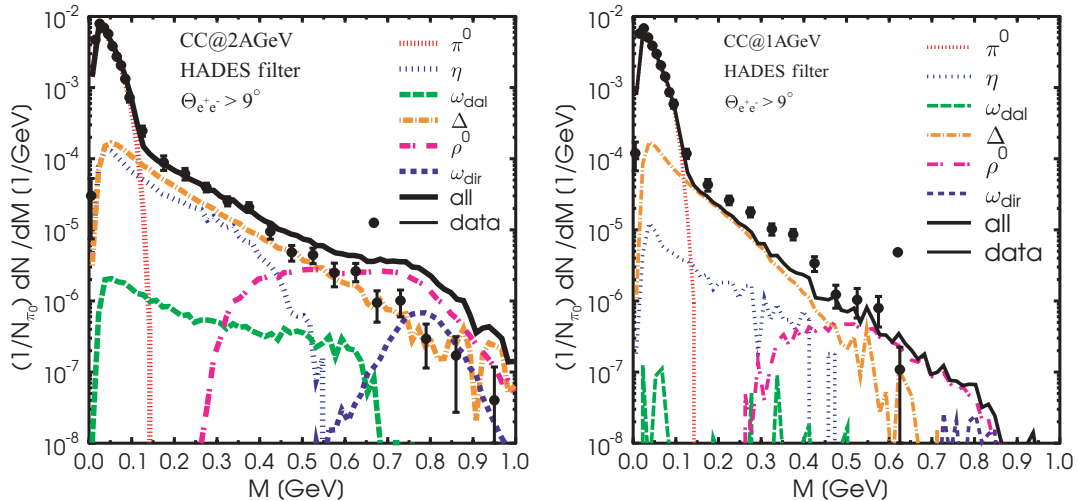


FIG. 6. (Color online) UrQMD model calculations for dilepton spectra from C+C collisions at beam energies of 2A GeV (left) and 1A GeV (right) in comparison to HADES data [26]. The different color lines display individual channels in the transport calculation, as indicated in the legend.

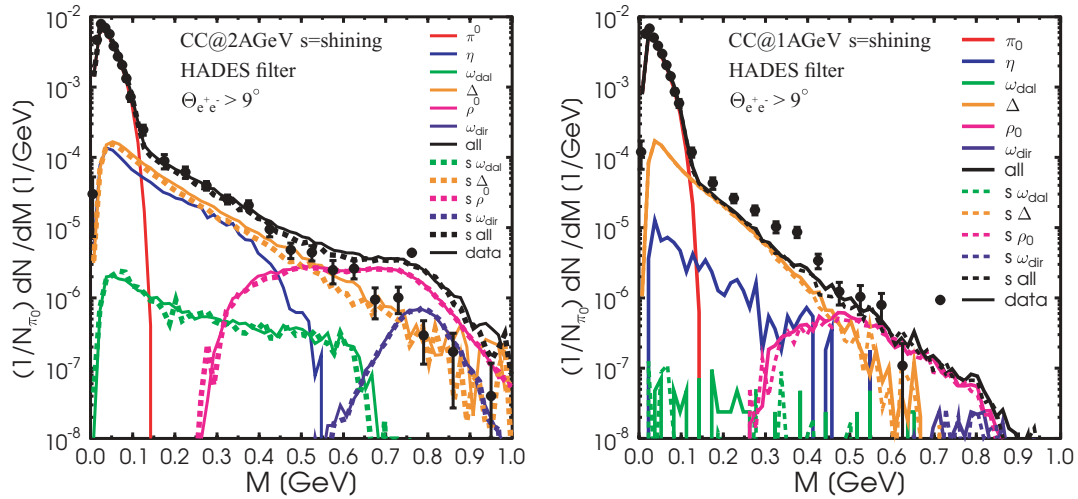


FIG. 7. (Color online) UrQMD model calculations for dilepton spectra from C+C collisions at beam energies of 2A GeV (left) and 1A GeV (right) in comparison to HADES data [26]. The full lines correspond to determination of the dilepton yield at the decay vertex of the parent particle. The dashed lines correspond to the dilepton yield resulting from the application of the shining method. The different color lines display individual channels in the transport calculation, as indicated in the legend, with s indicating the shining method.

2A GeV resulted in an overestimation of the data in the region of the vector-meson peak. However, the enhancement being more localized around the peak than in our case and about a factor of 1.5 lower at $M \sim m_{\text{peak}}$. The difference lies in the contribution originating from the direct ρ meson decay, suggesting a probably different value of ρ -meson multiplicity.

The spectrum obtained assuming that dileptons are emitted at the decay vertex of the parent resonance is shown in Fig. 7 and compared to the result of Fig. 6. The two results present no sizable differences, indicating that the methods to extract dileptons are essentially equivalent when looking at time integrated yields at low energies. The reason for that lies in the

smallness of the yield originating from reabsorbed resonances if compared to the emission from decaying resonances [33]. Note that no explicitly density-dependent medium modifications, such as, e.g., density-dependent parametrizations of in-medium masses, widths, and cross sections, are included in the present analysis. In Ref. [32] it has been argued that some differences between the two methods may arise when these effects are included, because only within the shining method the full in-medium dynamics of the vector meson is mapped to the dilepton emission history. The effect of absorption processes on the dilepton spectrum is analyzed in the Sec. VII.

Unfortunately no inclusive data on ρ -meson production cross section are available at the energy interesting for this work. Whether the observed overestimation of the HADES data is due to an overestimation of the ρ -meson multiplicities from the nucleon-nucleon collisions, the lack of a full treatment

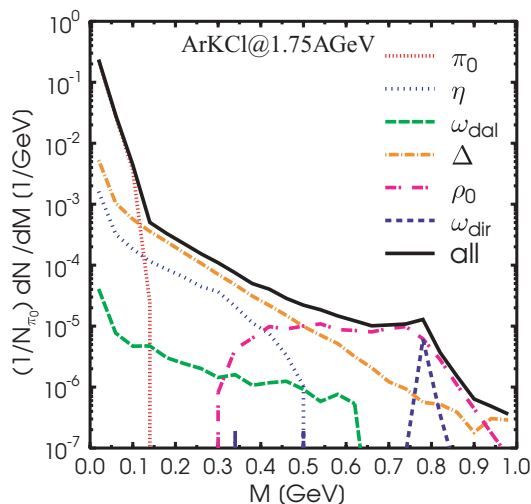


FIG. 8. (Color online) UrQMD model calculations for dilepton invariant mass spectra from Ar+KCl collisions at beam energy of 1.75A GeV. The calculations were performed with the shining method.

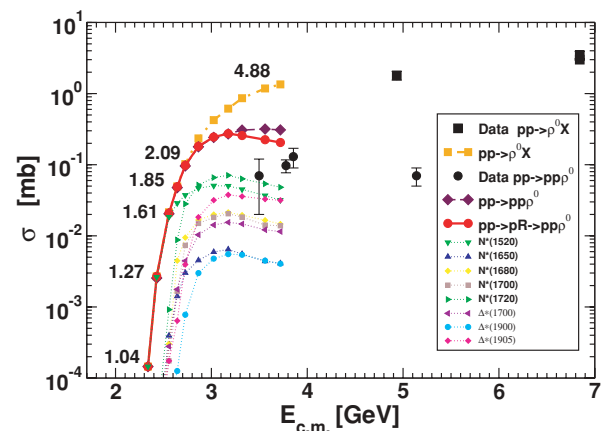


FIG. 9. (Color online) Same as described in the caption to Fig. 3 but for a smaller value of the $pp \rightarrow p\Delta^*$ and $pp \rightarrow pN^*$ cross sections, as explained in the text.

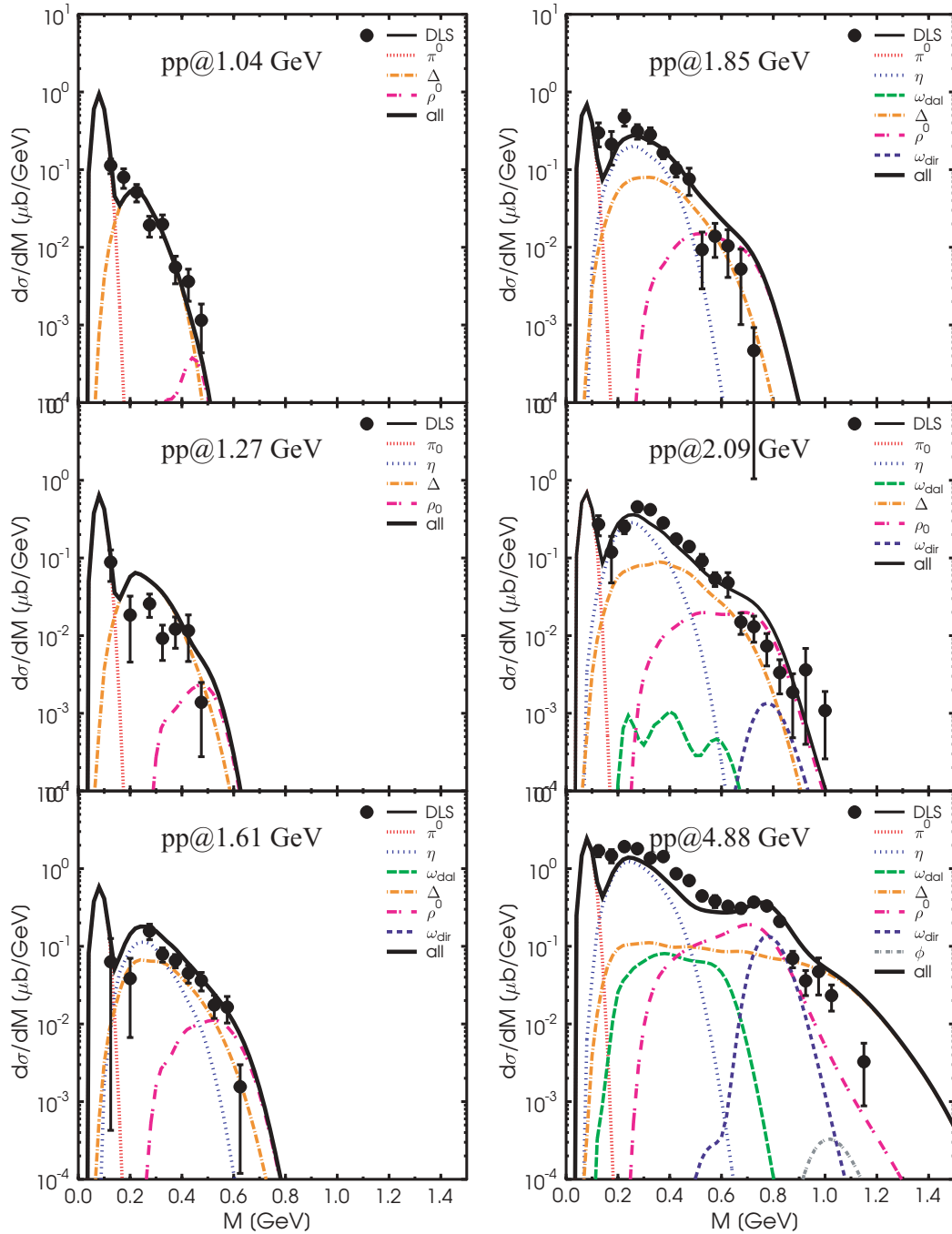


FIG. 10. (Color online) Same as described in the caption to Fig. 4 but for a smaller value of the $pp \rightarrow p\Delta^*$ and $pp \rightarrow pN^*$ cross sections.

of the in-medium properties in the present approach, or both cannot be decided on the basis of this experimental data. A comparison of the mass differential dilepton cross section for pp reactions to existing DLS data has been performed and discussed in the previous section. The analysis suggested that the meson multiplicity might be indeed slightly overshoot. Due to the low resolution of the DLS data, it is for the moment not possible to make exact quantitative conclusions. In this respect, the forthcoming HADES data on dilepton production in elementary reactions will be extremely helpful to indirectly constrain vector-meson multiplicities.

At 1A GeV a systematic underestimation of the data is observed in the mass region $0.2 < M < 0.4$ GeV with a maximum discrepancy at $M \approx 0.38$ GeV. The result is qualitatively in line with previous investigations of dilepton production in 1A GeV nucleus-nucleus collisions that link back in time to the DLS era [20,21,23]. Quantitatively, however, the discrepancy between the theoretical and experimental spectra spans here between factors of 1.5 and 2 from $M = 0.225$ GeV to $M = 0.325$ and is then at most of a factor of 3 at $M = 0.375$ GeV, whereas discrepancies of a factor of 4 had emerged from the studies performed in

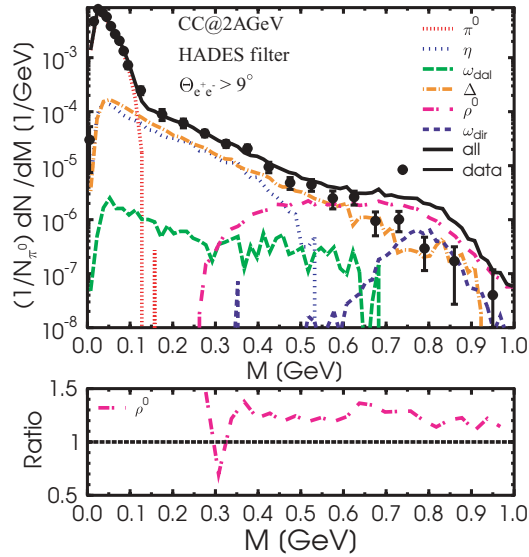


FIG. 11. (Color online) (Upper panel) Same as described in the caption to Fig. 6 but for a smaller value of the $pp \rightarrow p\Delta^*$ and $pp \rightarrow pN^*$ cross sections. (Lower panel) Ratio between the ρ^0 contribution to the dilepton spectra of Fig. 6 and Fig. 11.

the 1990s [20,21]. Enhanced bremsstrahlung cross sections in line with one-boson-exchange calculations by Kaptari and Kämpfer [63] have been recently proposed as possible explanation of the DLS puzzle [32]. The issue is, however, quite controversial. For pn reactions the cross sections of Ref. [63] differ up to a factor of 4 from previous calculations [64,65]. In Ref. [63] and [65] the same couplings have been used, but differences can originate due to a different prescription used by the groups to restore gauge invariance in the effective theory. Because the way this restoration can be achieved is not unique, there are no straight arguments that favor one calculation over the other. To investigate this

discrepancy, dilepton production in nucleon-nucleon collisions has been recently revisited within a fully relativistic and gauge-invariant framework [66]. For the various contributions analyzed— pp bremsstrahlung, pn bremsstrahlung, as well as contributions with the Δ isobar intermediate state—the authors of Ref. [66] found cross sections smaller than those in Ref. [63]. In pn collisions at beam energies of 1.04 and 2.09 GeV, in particular, differences in the bremsstrahlung contribution by factors of between 2 and 3 were found. Future HADES measurements of dilepton spectra in elementary, especially pn , collisions will help to shed light into this new puzzle.

V. PREDICTIONS FOR Ar+KCL

In this section we consider the reaction Ar+KCl at 1.75A GeV, recently measured and currently analyzed by the HADES Collaboration. The predictions presented here refer to minimum bias calculations and have been obtained adopting the shining method. All spectra are normalized to the pion multiplicity.

The invariant mass differential dilepton spectrum is shown in Fig. 8. Compared to C+C at 2A GeV we observe a smaller contribution of the η resonances relatively to the e^+e^- -pairs originating from the Δ Dalitz decay. Up to a dilepton mass of 0.4 GeV the biggest contribution to this mass spectrum occurs from the long-lived mesons η and π^0 and the baryonic resonance Δ . Considering the contribution originating from vector mesons it is visible that the ω Dalitz decay again plays only a subordinate role, while the e^+e^- pair production from ω direct decay becomes important for higher invariant mass, such that in the (unfiltered) dilepton spectrum a peak at $M \approx 0.8$ GeV is visible. The direct decay of the vector meson ρ dominates the mass spectrum for $M > 0.5$ GeV.

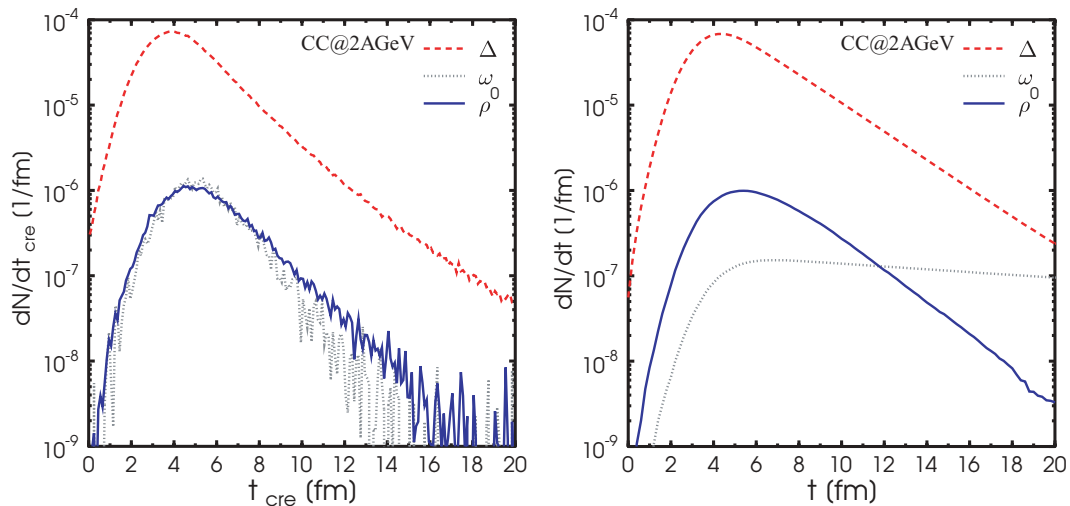


FIG. 12. (Color online) Dilepton multiplicity for minimal bias C+C collisions at beam energies of 2A GeV as a function of the time at which the parent particle made its first appearance in the evolving system (left panel) and corresponding averaged dilepton rate as a function of the evolution time of the heavy-ion collision (right panel).

VI. INVESTIGATING EFFECTS OF BARYON RESONANCE PRODUCTION CROSS SECTION

In this section we investigate the effect that an eventual overestimation of the $pp \rightarrow p\Delta^*$ and $pp \rightarrow pN^*$ cross sections would have on the ρ^0 meson and, consequently, dilepton production. The main concern is to understand whether the main features of the results presented by far will be altered and where more experimental input is needed. However, for the results presented in this work (apart from this section) the cross sections presented in Fig. 3 are used.

Due to the lack of high-quality data and to explore the effects of this change, we divide all $pp \rightarrow p\Delta^*$ and $pp \rightarrow pN^*$ cross sections by a factor of 3 with exception for the $pp \rightarrow pN^*(1535)$ cross section that is constrained by η production. This procedure is surely too crude but provides a rough estimate of the consequences that an eventual insufficient modeling of the hitherto used $pp \rightarrow p\Delta^*$ and $pp \rightarrow pN^*$ cross sections might have on the model calculations for dilepton spectra. The results obtained with the modified values of the $pp \rightarrow p\Delta^*$ and $pp \rightarrow pN^*$ cross sections are shown in Fig. 9 and Fig. 10. We observe that the model calculations of the exclusive ρ^0 -meson production cross sections moves closer to the experimental data and the DLS data are well described in all mass ranges. In particular, the peak previously observed in the dilepton spectra for pp collisions at 2.09 GeV vanishes to a large extent. We note that the readjustment of the exclusive production of the ρ^0 meson only weakly alters the inclusive production at a laboratory energy of 4.88 GeV, as well as the respective result for the dilepton spectra.

However, the main features of our results remain. In particular, the contribution to the dilepton spectrum from ρ^0 mesons at the lowest energies, although reduced, is still visible and distinguishable. Concerning the reaction C+C at 2A GeV, we observe that the HADES data remain overestimated in the peak region even when the readjusted cross sections are used, as shown in Fig. 11. Many processes, such as multiple scattering, backward reactions, Fermi motion, etc., distinguish a heavy-ion collision from a simple superposition of elementary reactions occurring at the same beam energy. It is also clear that in the local equilibrium limit particle production would be statistical and information on the employed elementary cross sections would be lost. In the present case, which can be seen as an intermediate regime between the two limiting cases of an elementary reaction and an equilibrated system, we find that a small readjustment of some particular cross sections can still affect the dilepton spectrum, but the differences are smaller than in the elementary case.

VII. TRACING THE DILEPTON EMISSION BACK IN TIME

In this section we investigate the dependence of the dilepton signal on the reaction evolution time including the corresponding densities. The aim of this analysis is to trace the dilepton emission in time to identify the different stages and density regimes of the heavy-ion collision from which dileptons originate. The study is performed for minimum bias C+C reactions at 2A GeV.

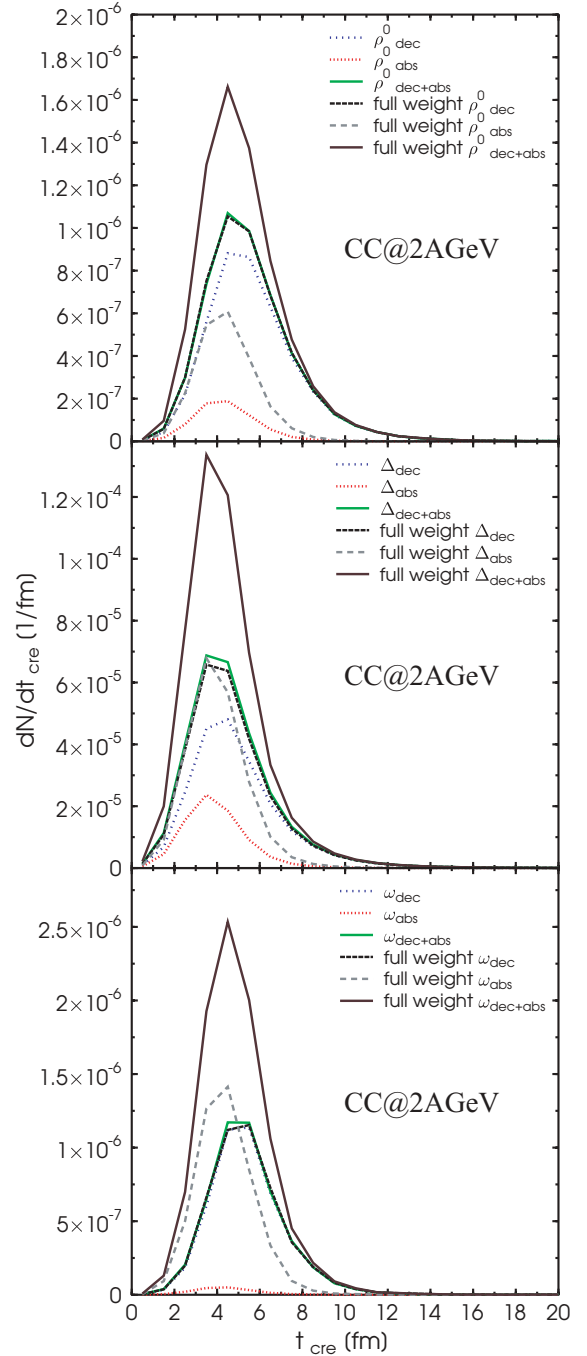


FIG. 13. (Color online) Dilepton multiplicity from minimal bias C+C collisions at beam energies of 2A GeV as a function of the time at which the parent particle made its first appearance in the evolving system. The dashed lines denote calculation where the full branching ratio into dileptons is attached to both the decay and the absorption vertices.

Let us focus our discussion on the contributions of the vector mesons and the Δ resonance. The remaining contributions, π^0 and η Dalitz decays, although large, do not play a central role in the physics one aims to explore with dilepton experiments and can be viewed as some sort of standard “background.” The left panel of Fig. 12 shows the dilepton

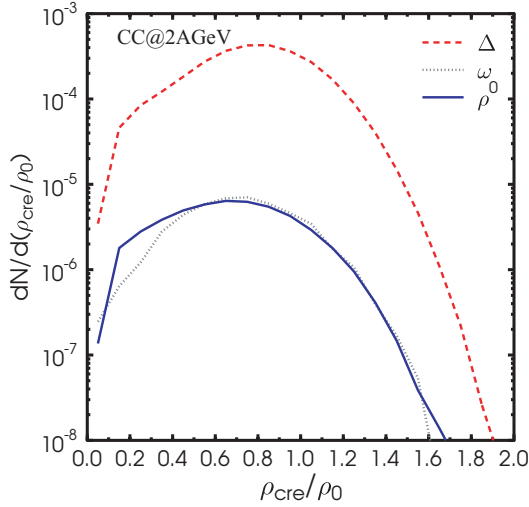


FIG. 14. (Color online) Dilepton multiplicity from minimal bias C+C collisions at beam energies of 2A GeV as a function of the local density present in the space-time point at which the parent particle has been created.

multiplicities as a function of the time at which the parent particle has been created. In the right panel, the multiplicities are shown as a function of the evolution time of the heavy-ion reaction. In the latter, the continuous emission of dileptons from the parent particle is explicitly shown, whereas in the former the integrated value is shown. In other words, from a particle that lives from time t_i until time t_f , dileptons are emitted with rate

$$\frac{dN^{e^+e^-}(t)}{dt} = \begin{cases} \Gamma^{e^+e^-}/\gamma & \text{for } t_i \leq t \leq t_f \\ 0 & \text{otherwise.} \end{cases} \quad (16)$$

Here t denotes the time in the frame of the evolving system (center-of-mass frame of the nucleus-nucleus collision). The Lorentz factor γ connects a time interval in this system to the corresponding one in the rest frame of the emitting particle. For each particle, the function of t (16) is plotted in the right panel of Fig. 12 and corresponds to a straight line going from t_i to t_f . The corresponding integral

$$\int_{t_i}^{t_f} \frac{dN^{e^+e^-}(t)}{dt} dt = \Gamma^{e^+e^-} \tau, \quad (17)$$

where $\tau = (t_f - t_i)/\gamma$ is the lifetime of the particle, gives the total number of dilepton emitted by the particle (created at $t = t_i$) and is reported in the left panel of Fig. 12.

We observe that:

- (i) Most dileptons originate from particles created within the first 8 fm. The emission is maximal from vector mesons created at about 5 fm and Δ resonances created at slightly earlier time (about 3.5 fm). This is understandable if one considers that in the resonance model vector mesons arise from the decay of baryonic resonances. Because the baryonic resonances have a typical total width of the order of 100–200 MeV, their decay takes typically place about 1–2 fm after their creation.

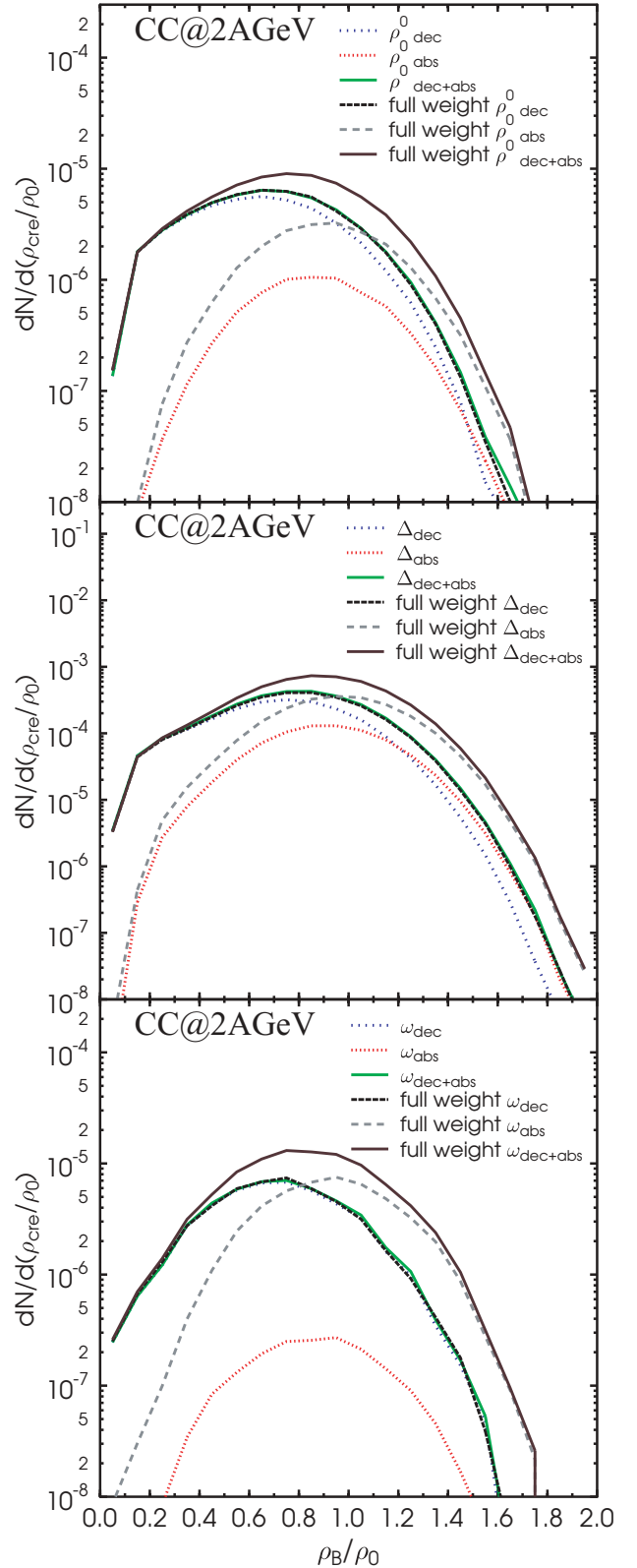


FIG. 15. (Color online) Dilepton multiplicity from minimal bias C+C collisions at beam energies of 2A GeV as a function of the local density present in the space-time point at which the parent particle has been created. The dashed lines denote calculation where the full branching ratio into dileptons is attached to both the decay and the absorption vertices.

- (ii) In the case that the parent particles is a relatively short-lived particle, e.g., a Δ resonance or a ρ meson, most dileptons are emitted within the first 10 fm, with a maximum around 6 fm. Later, for $t > 6$ fm, the dilepton emission strongly decreases with increasing time. On the contrary, if the parent particle is a long-lived particle, e.g., a ω meson, dileptons are emitted continuously at an almost constant rate for $t > 6$ fm. This is due to the fact that those ω mesons that happened to survive the various absorption processes live relatively long and emit dileptons during their whole lifetime.

In Fig. 13 the role of absorption on the reduction of the dilepton signal is shown. The observed yield is compared to the yield expected from a vacuumlike picture in which the parent resonance, after being produced, does not interact further up to its decay, here simply denoted by “full weight” scenario. For a detailed discussion of the different prescriptions for dilepton production, see Ref. [33]. The total dilepton signal from vector mesons is reduced by a factor of 1.5 (for the ρ meson) to 2 (for the ω meson) due to reabsorption. Especially in the case of the ω meson, the “potential” dilepton signal of those particles that are absorbed (labeled by ω_{abs} in Fig. 13) is strongly suppressed (by a factor of 20).

Next, we investigate the influence of the baryon density locally present on the electromagnetic response of the system, as depicted in Fig. 14. It is clear that a particle propagating through a high-density zone of the system will interact, with a certain probability, with the particles present in its surroundings. Absorptive interactions, e.g., $\rho N \rightarrow N^*(1520)$, will lead to the disappearance of the parent particle from the system within shorter times than its vacuum mean lifetime (determined by its decay width). As a consequence of its shorter lifetime, the total dilepton yield from the particle will be reduced with respect to the yield expected if the particle would be present in the system until its decay and emit dileptons for a time interval τ_{dec} . In particular, the number of dileptons expected to be emitted by a parent particle created in a space-time point characterized by a local baryon density ρ_{cre} is analyzed. The result is reported in Fig. 15.

We observe that between 13% and 20% of dileptons originate from particles created at densities $\rho_{\text{cre}} > \rho_0$ and that absorption reduces the potential dilepton yield from these particles by a factor of 1.5. This effect is particularly strong in the case of the ω meson. It is evident from the previous analysis that the parent particles seem to be characterized by relatively short lifetimes in the high-density phase.

VIII. SUMMARY AND CONCLUSION

Dilepton production in nucleus-nucleus and proton-proton reactions at SIS/BEVALAC energies has been analyzed within the microscopic transport model UrQMD. The results for invariant mass differential dilepton spectra have been compared to HADES data for C+C collisions at 1A GeV and 2A GeV and to DLS data for pp reactions. Additionally, predictions for dilepton spectra in pp reactions at 1.25, 2.2, and 3.5 GeV as well as in Ar+KCl at 1.78A GeV have been presented. The analysis shows that the low-mass region of the dilepton spectra for C+C collisions is slightly underestimated by the model calculations at 1A GeV but well described at 2A GeV.

The dilepton emission was analyzed in its dependence on the evolution time and densities typical for the regime probed by the HADES experiment. In particular, the influence of absorption of the parent resonances on their dilepton emission has been discussed. We found that absorption is responsible for a global suppression of the dilepton signal of factors of about 1.5–2. The absorption processes are more copious in the high-density phase, resulting in a stronger suppression for particles (and therefore dileptons) produced at the highest densities.

ACKNOWLEDGMENTS

We thank Y. Pachmayer for providing the experimental data and the HADES filter for the reaction C+C at 1A GeV, and E. L. Bratkovskaya for discussions on the ρ -meson production cross section. This work was supported by BMBF, GSI, DFG, and the Hessen Initiative for Excellence (LOEWE) through the Helmholtz International Center for FAIR (HIC for FAIR). We thank the Center for Scientific Computing for providing computational resources.

-
- [1] L. H. Xia, C. M. Ko, L. Xiong, and J. Q. Wu, Nucl. Phys. **A485**, 721 (1988).
 [2] L. H. Xia, C. M. Ko, and C. T. Li, Phys. Rev. C **41**, 572 (1990).
 [3] G. Wolf, G. Batko, W. Cassing, U. Mosel, K. Niita, and M. Schaefer, Nucl. Phys. **A517**, 615 (1990).
 [4] G. Wolf, W. Cassing, U. Mosel, and M. Schaefer, Phys. Rev. C **43**, R1501 (1991).
 [5] G. Wolf, W. Cassing, and U. Mosel, Prog. Part. Nucl. Phys. **30**, 273 (1993) [Nucl. Phys. **A552**, 549 (1993)].
 [6] M. Asakawa, C. M. Ko, P. Levai, and X. J. Qiu, Phys. Rev. C **46**, R1159 (1992).
 [7] M. A. Mazzone (HELIOS/3 Collaboration), Nucl. Phys. **A566**, 95C (1994).
 [8] G. Q. Li and C. M. Ko, Nucl. Phys. **A582**, 731 (1995).
 [9] W. Cassing, W. Ehehalt, and C. M. Ko, Phys. Lett. **B363**, 35 (1995).
 [10] C. Song and C. M. Ko, Phys. Rev. C **53**, 2371 (1996).
 [11] G. Agakichiev *et al.* (CERES Collaboration), Phys. Rev. Lett. **75**, 1272 (1995); A. Drees, Nucl. Phys. **A610**, 536C (1996).
 [12] G. Q. Li, C. M. Ko, and G. E. Brown, Phys. Rev. Lett. **75**, 4007 (1995).
 [13] G. Chanfray, R. Rapp, and J. Wambach, Phys. Rev. Lett. **76**, 368 (1996); R. Rapp and J. Wambach, Adv. Nucl. Phys. **25**, 1 (2000).
 [14] C. M. Ko, G. Q. Li, G. E. Brown, and H. Sorge, Nucl. Phys. **A610**, 342C (1996).
 [15] G. Q. Li, C. M. Ko, G. E. Brown, and H. Sorge, Nucl. Phys. **A611**, 539 (1996).

- [16] R. Rapp, G. Chanfray, and J. Wambach, Nucl. Phys. **A617**, 472 (1997).
- [17] B. Friman and H. J. Pirner, Nucl. Phys. **A617**, 496 (1997).
- [18] W. Cassing, E. L. Bratkovskaya, R. Rapp, and J. Wambach, Phys. Rev. C **57**, 916 (1998).
- [19] R. J. Porter *et al.* (DLS Collaboration), Phys. Rev. Lett. **79**, 1229 (1997).
- [20] E. L. Bratkovskaya, W. Cassing, R. Rapp, and J. Wambach, Nucl. Phys. **A634**, 168 (1998).
- [21] C. Ernst, S. A. Bass, M. Belkacem, H. Stoecker, and W. Greiner, Phys. Rev. C **58**, 447 (1998).
- [22] E. L. Bratkovskaya and C. M. Ko, Phys. Lett. **B445**, 265 (1999).
- [23] K. Shekhter, C. Fuchs, A. Faessler, M. Krivoruchenko, and B. Martemyanov, Phys. Rev. C **68**, 014904 (2003).
- [24] R. Arnaldi *et al.* (NA60 Collaboration), Phys. Rev. Lett. **96**, 162302 (2006).
- [25] D. Adamova *et al.*, Phys. Lett. **B666**, 425 (2008).
- [26] G. Agakichiev *et al.* (HADES Collaboration), Phys. Rev. Lett. **98**, 052302 (2007).
- [27] G. Agakishiev *et al.* (HADES Collaboration), Phys. Lett. **B663**, 43 (2008).
- [28] M. D. Cozma, C. Fuchs, E. Santini, and A. Fassler, Phys. Lett. **B640**, 170 (2006).
- [29] D. Schumacher, S. Vogel, and M. Bleicher, Acta Phys. Hung. A **27**, 451 (2006).
- [30] M. Thomere, C. Hartnack, G. Wolf, and J. Aichelin, Phys. Rev. C **75**, 064902 (2007).
- [31] J. Ruppert, C. Gale, T. Renk, P. Lichard, and J. I. Kapusta, Phys. Rev. Lett. **100**, 162301 (2008).
- [32] E. L. Bratkovskaya and W. Cassing, Nucl. Phys. **A807**, 214 (2008).
- [33] S. Vogel, H. Petersen, K. Schmidt, E. Santini, C. Sturm, J. Aichelin, and M. Bleicher, Phys. Rev. C **78**, 044909 (2008).
- [34] E. Santini, M. D. Cozma, A. Faessler, C. Fuchs, M. I. Krivoruchenko, and B. Martemyanov, Phys. Rev. C **78**, 034910 (2008).
- [35] G. E. Brown and M. Rho, Phys. Rev. Lett. **66**, 2720 (1991).
- [36] T. Hatsuda and S. H. Lee, Phys. Rev. C **46**, R34 (1992).
- [37] W. Peters, M. Post, H. Lenske, S. Leupold, and U. Mosel, Nucl. Phys. **A632**, 109 (1998); M. Post, S. Leupold, and U. Mosel, Nucl. Phys. **A689**, 753 (2001); M. Post, S. Leupold, and U. Mosel, Nucl. Phys. **A741**, 81 (2004).
- [38] M. F. M. Lutz, G. Wolf, and B. Friman, Nucl. Phys. **A706**, 431 (2002) [Erratum-*ibid.* **A765**, 495 (2006)].
- [39] J. Aichelin and H. Stöcker, Phys. Lett. **B176**, 14 (1986); H. Sorge, H. Stöcker, and W. Greiner, Ann. Phys. **192**, 266 (1989); J. Aichelin, Phys. Rep. **202**, 233 (1991).
- [40] S. A. Bass, C. Hartnack, H. Stöcker, and W. Greiner, Phys. Rev. C **51**, 3343 (1995).
- [41] L. A. Winkelmann *et al.*, Nucl. Phys. **A610**, 116c (1996).
- [42] W. M. Yao *et al.* (Particle Data Group), J. Phys. G **33**, 1 (2006).
- [43] C. Sturm *et al.* (KaoS Collaboration), Phys. Rev. Lett. **86**, 39 (2001).
- [44] S. A. Bass *et al.*, Prog. Part. Nucl. Phys. **41**, 255 (1998).
- [45] M. Bleicher *et al.*, J. Phys. G **25**, 1859 (1999).
- [46] H. Petersen, M. Bleicher, S. A. Bass, and H. Stöcker, arXiv:0805.0567 [hep-ph].
- [47] L. A. Winkelmann, H. Sorge, H. Stöcker, and W. Greiner, Phys. Rev. C **51**, R9 (1995).
- [48] M. Post and U. Mosel, Nucl. Phys. **A688**, 808 (2001).
- [49] R. Holzmann *et al.* (TAPS Collaboration), Phys. Rev. C **56**, R2920 (1997).
- [50] H. Calen *et al.*, Phys. Rev. C **58**, 2667 (1998).
- [51] S. Teis, W. Cassing, M. Effenberger, A. Hombach, U. Mosel, and G. Wolf, Z. Phys. A **356**, 421 (1997).
- [52] R. Averbeck *et al.* (TAPS Collaboration), Z. Phys. A **359**, 65 (1997).
- [53] V. Flaminio, W. G. Moorhead, D. R. O. Morrison, and N. Rivoire, CERN-HERA Report No. 84-01, 1984.
- [54] L. G. Landsberg, Phys. Rep. **128**, 301 (1985).
- [55] P. Koch, Z. Phys. C **57**, 283 (1993).
- [56] A. Faessler, C. Fuchs, and M. I. Krivoruchenko, Phys. Rev. C **61**, 035206 (2000).
- [57] E. L. Bratkovskaya, W. Cassing, M. Effenberger, and U. Mosel, Nucl. Phys. **A653**, 301 (1999).
- [58] M. I. Krivoruchenko and A. Faessler, Phys. Rev. D **65**, 017502 (2001).
- [59] U. W. Heinz and K. S. Lee, Nucl. Phys. **A544**, 503 (1992).
- [60] W. K. Wilson *et al.* (DLS Collaboration), Phys. Rev. C **57**, 1865 (1998).
- [61] A. Faessler, C. Fuchs, M. I. Krivoruchenko, and B. V. Martemyanov, J. Phys. G **29**, 603 (2003).
- [62] S. Vogel and M. Bleicher, Phys. Rev. C **74**, 014902 (2006).
- [63] L. P. Kaptari and B. Kampfer, Nucl. Phys. **A764**, 338 (2006).
- [64] M. Schafer, T. S. Biro, W. Cassing, and U. Mosel, Phys. Lett. **B221**, 1 (1989).
- [65] R. Shyam and U. Mosel, Phys. Rev. C **67**, 065202 (2003).
- [66] R. Shyam and U. Mosel, Phys. Rev. C **79**, 035203 (2009).